ACES Asian Chemical Editorial Society

DOI: 10.1002/asia.201600675

CHEMISTRY AN ASIAN JOURNAL Full Paper

Polycyclic Aromatic Hydrocarbons

Highly Contorted 1,2,5-Thiadiazole-Fused Aromatics for Solution-Processed Field-Effect Transistors: Synthesis and Properties

Xin Shi[+],[a] Shuli Liu[+],[a] Chunming Liu,[b] Yueming Hu,[a] Saihua Shi,[a] Nina Fu,[a] Baomin Zhao,*[a] Zhaohui Wang,*[b] and Wei Huang*[a, c]

Abstract: A straightforward strategy has been used to construct 1,2,5-thiadiazole-fused 12-ring π systems through two-fold Stille coupling and subsequent cyclodehydrogenation by utilizing the building blocks of naphthodithiophene and 5,6-substituted benzo[*b*]-2,1,3-thiadidazole. Molecules **1a** and **1b**, which exhibit highly contorted π surfaces, show a butterfly-shaped conformation according to DFT calculations. Within the molecules, a plane-to-plane angle of 44.8° was found. UV/Vis absorption, thermogravimetric analysis, differential scanning calorimetry, and cyclic voltammetry (CV) were used to study their physical properties. Strong intermolecular interactions of the nonplanar molecules were also observed by concentration-dependent ^{1}H NMR spectroscopy measurements and thin-film XRD characterization. The low-lying LUMO and high-lying HOMO levels of the molecules are −3.73 and −5.48 eV, respectively, as estimated from CV measurements; this indicates their potential as semiconducting materials for solution-processed organic field-effect transistors (OFETS). A field-effect hole mobility of up to 0.035 $cm^2V^{-1}s^{-1}$, a threshold voltage of 6.98 V, and a current on/off ratio of 8.65×10^5 in air for **1a** have been demonstrated with the top-contact bottom-gate field-effect transistor device structures; this represents an important step toward the solution-processed OFET application of contorted aromatics.

Introduction

Organic semiconductors are of great importance and interest from the viewpoint of their fundamental electronic and optoelectronic properties and their potential applications in organic electronics, such as organic field-effect transistors (OFETs).[1,2] During recent decades, remarkable progress in the performance of OFETs has been achieved.[3–5] For example, state-of-the-art charge-carrier mobilities for thin-film OFETs are 19.3 $cm^2V^{-1}s^{-1}$ in the case of vacuum-deposited small molecules,[6] 31.3 $cm^2V^{-1}s^{-1}$ for solution-processed small molecules,[7] and 11.4 $cm^2V^{-1}s^{-1}$ for conjugated polymers.[8] This impressive accomplishment was mainly achieved by the molecular engineering of the structures of organic semiconductors, assisted by great successes in device fabrication techniques.[9–11] Decades of research into OFET materials has rationalized the design principles of materials towards high charge mobilities, including an extended π-conjugated system, structural symmetricity, and planarity.[12–14] Fusing aromatic rings to give polycyclic aromatic hydrocarbons (PAHs) is an effective strategy toward large and rigid aromatic structures.[15,16] The rigidity of fused aromatic structures helps to reduce reorganization energy, thereby increasing the rate of electron transfer.[3,11] Furthermore, planar aromatic structures have the ability to pack tightly in the solid state, often leading to desirable π–π interactions.[10,15]

Since the remarkable performance of pentacene in OFETs was discovered,[17] the chemistry of larger linear acenes has recently been aggressively developed.[13,14,16] Thus, π conjugation in most organic semiconductors for OFETs is extended through 1D condensation of aromatic rings. On the other hand, π-extension systems with 2D conjugation for field-effect transistor (FET) devices have not been extensively developed.[18–25] Although the performances of 2D PAHs were not as remarkable as those of 1D acenes, it is worth paying them much attention.

[a] *X. Shi,[+] S. Liu,[+] Y. Hu, S. Shi, Dr. N. Fu, Dr. B. Zhao, Prof. Dr. W. Huang*
Key Laboratory for Organic Electronics and Information Displays
Institute of Advanced Materials (IAM), Jiangsu National
Synergetic Innovation Center for Advanced Materials (SICAM)
Nanjing University of Posts and Telecommunications
9 Wenyuan Road, Nanjing 210023 (P.R. China)
E-mail: iambmzhao@njupt.edu.cn

[b] *C. Liu, Prof. Dr. Z. Wang*
Beijing National Laboratory for Molecular Sciences
Key Laboratory of Organic Solids, Institute of Chemistry
Chinese Academy of Sciences, Beijing 100190 (P.R. China)
E-mail: wangzhaohui@iccas.ac.cn

[c] *Prof. Dr. W. Huang*
Key Laboratory of Flexible Electronics (KLOFE)
Institute of Advanced Materials (IAM), Jiangsu National
Synergetic Innovation Center for Advanced Materials (SICAM)
Nanjing Tech University (Nanjing Tech)
30 South Puzhu Road, Nanjing 211816 (P.R. China)
E-mail: wei-huang@njtech.edu.cn
iamdirector@fudan.edu.cn

[+] *These authors contributed equally to this work.*

*Supporting information for this article can be found under http://dx.doi.org/10.1002/asia.201600675. It contains NMR spectra, MALDI-TOF MS spectra, DFT data, AFM images, and SEM images of **1a**.*

Because 2D PAHs can be constructed through the straightforward strategy of chemical oxidant induced dehydrogenation steps (namely, the Scholl reaction).[18–22] The Scholl reaction has been extensively utilized for the synthesis of planar PAHs.[15,26] Importantly, the oxidative cyclodehydrogenation reaction can be accomplished under ambient conditions in high yields by using a variety of "mean metal" oxidants, such as $FeCl_3$ in dichloromethane,[26–28] $CuCl_2$ or copper(II) triflate ($Cu(OTf)_2$), and $AlCl_3$.[29] Pei and co-workers reported the preparation of BN-embedded heterosuperbenzenes, which exhibited p-channel characteristics, with the highest mobility of 0.23 $cm^2V^{-1}s^{-1}$, a low threshold of -3 V, and a current on/off ratio of $>10^4$.[30] It should be mentioned that 2D PAHs are expected to afford unusual nano- or microribbons. These micro-/nanoribbons can be applied in solution-processed OFETs to give mobilities as high as 12.6 $cm^2V^{-1}s^{-1}$.[31]

Mobility enhancement and environmental robustness to oxidation in ambient air are two major requirements of organic semiconductors for OFETs.[3,14] The general approaches to achieve stable semiconductors with desirable band gaps and energy levels include 1) introducing electron-withdrawing substituents (e.g., fluorine[32] or carboximide[33]) onto the traditional acenes, and/or 2) replacement carbon atoms within the π system by electron-deficient atoms (e.g., imine nitrogen[14]). Recently, the electron-deficient heterocycle of thiadiazole has been used to afford 1,2,5-thiadiazole-fused compounds because this ring leads to several advantages, such as a high electron affinity, no steric repulsion between adjacent aromatic rings, and strong intra-/intermolecular interactions caused by short S···N contacts (see examples a–e in Figure 1).[34–38] However, few of them can be used as active materials for OFETs obtained by low-cost solution-processed techniques.

In this regard, we report the successful synthesis of 12-ring 1,2,5-thiadiazole-fused heteroacences **1a–b** (Figure 1) through twofold Stille coupling and subsequent cyclodehydrogenation by utilizing the building blocks of naphthodithiophene (NDT) and 5,6-substituted benzo[*b*]-2,1,3-thiadidazole (BT; Scheme 1). The target molecules can be considered as a combination of two dithienonaphtho–thiadiazoles (DTNTs)[36] and one NDT.[20] Different side chains on NDT were used for tuning their solubility and aggregation behavior in the solid state. In addition, lower-lying HOMO/LUMO levels were expected for these compounds. Their photophysical properties were studied by UV/Vis absorption both in solutions and as thin films. Their electrochemical properties were investigated by cyclic voltammetry (CV) and the corresponding energy levels were determined by a combination of the analysis of CV and absorption data. Their thermal behavior and self-assembly in the solid state were studied by thermogravimetric analysis (TGA), differential scanning calorimetry (DSC), and thin-film XRD measurements. The molecular geometry and π surface were studied with DFT calculations. Finally, charge transport has been studied in solution-processed OFET devices and is discussed in relation to the molecular properties.

Results and Discussion

Synthesis and Characterization of Materials

The synthesis of these BT-embedded 2D PAHs is depicted in Scheme 1. The central NDT derivatives[3] were obtained through the $FeCl_3$-mediated Scholl reaction in good yields.[26,27] The distannyl compounds of **4** were conveniently prepared in situ by lithiation of **3** with *n*BuLi in THF at $-78\,^{\circ}C$ followed by quenching with tributyltin chloride and aqueous workup; these compounds were used without further purification. 5,6-Dibromobenzothiadiazole was synthesized according to a procedure reported in the literature.[39] Compound **5** can be prepared through Stille coupling of 5-dodecyl-2-tributyl-stannylthiophene and 5,6-dibromo-BT in 35–40% yield.[40] However, the direct C–H arylation of 2-dodecylthiophene and 5,6-dibromo-BT is superior and proceeds in a good yield of 73%.[41] It was assumed that in the direct C–H arylation reaction the reactivity of the bromine atom was restricted after the other one was replaced by dodecylthiophene. The precursors of **6** were prepared by a Stille coupling reaction between **4** and **5** at a molar ratio of 1:2.2 in moderate yields. The $FeCl_3$ oxidative cyclization was then utilized to construct the 12-ring-fused skeleton through thienyl–thienyl carbon–carbon bond formation.[26] Compound **3** can be formed through the oxidization of **2** with

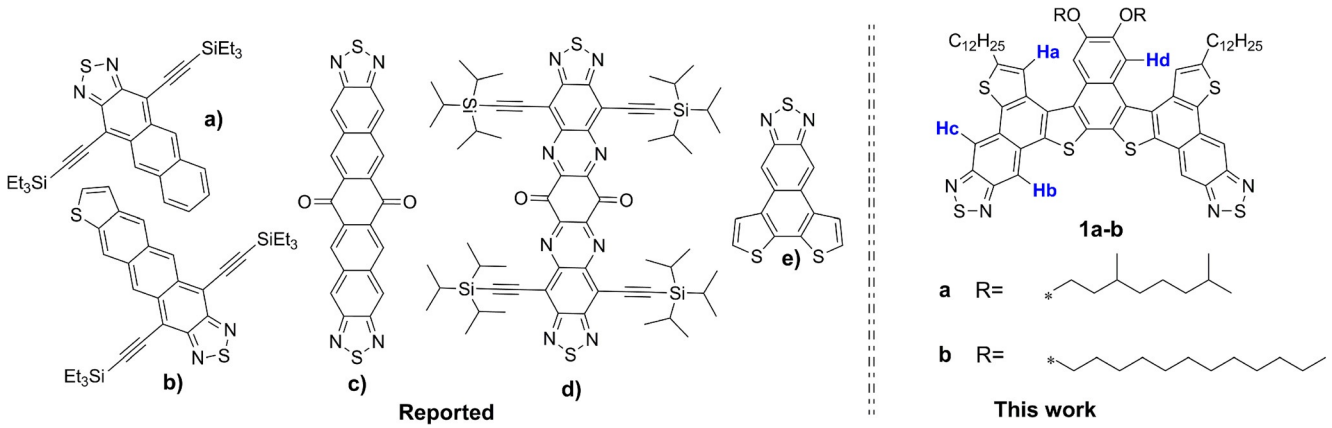

Figure 1. Molecular structures of 1,2,5-thiadiazole-fused aromatics, including **1a–b** (aromatic hydrogen atoms are highlighted).

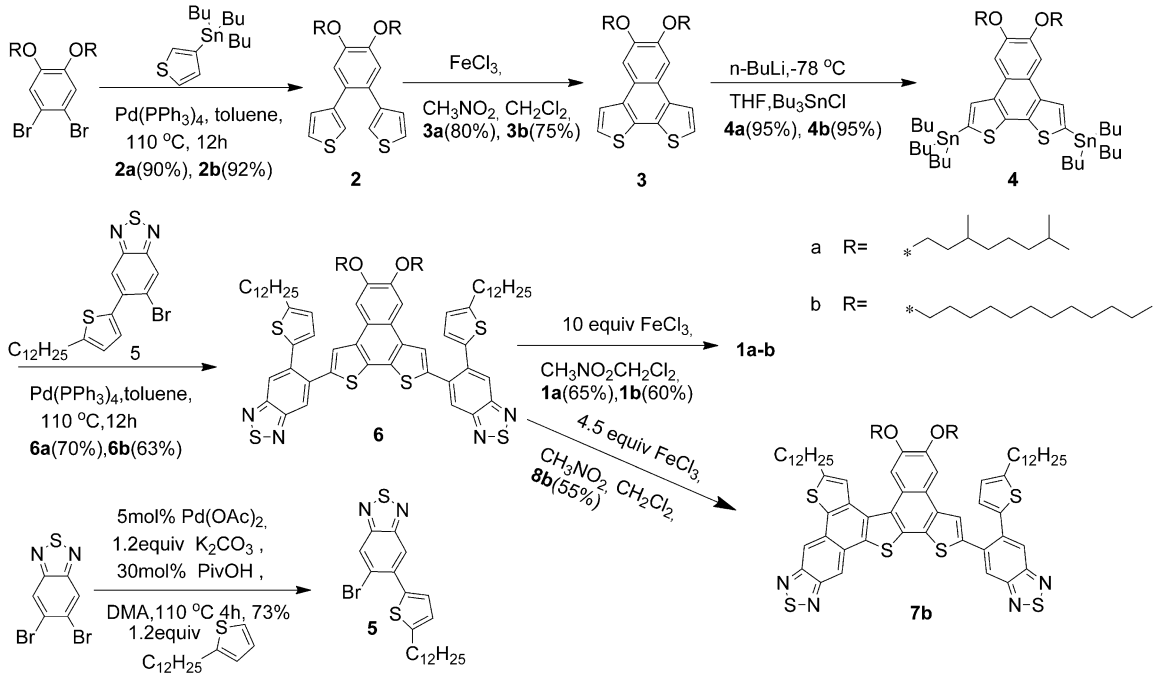

Scheme 1. Synthesis of **1a** and **1b**. THF = tetrahydrofuran, PivOH = pivalic acid, DMA = *N*,*N*′-dimethylacetamide.

2.2 equivalents of $FeCl_3$ in good yields (75–80%). However, the twofold Scholl annulation toward **1a–b** can only be accomplished by using 10 equivalents of $FeCl_3$ in our hands. With 4.5 equivalents of $FeCl_3$, only the unilateral fused intermediate **7b** was obtained, which was confirmed by ^{1}H NMR spectroscopy and MALDI-TOF mass spectrometry (Figure S22 in the Supporting Information). A plausible explanation for this is that the decreased activity of thiophene units is caused by the substituted BT units, which are electron deficient.

All compounds are readily dissolved in common organic solvents, such as dichloromethane, chloroform, THF, and toluene, and allow us to purify them by column chromatography. The structures of these compounds are identified by ^{1}H and ^{13}C NMR spectroscopy and MALDI-TOF mass spectrometry (see the Supporting Information). For example, ^{1}H NMR spectroscopy was employed to monitor the oxidative cyclization reactions. After cyclization, the resonance at $\delta \approx 6.88$ ppm, which could be assigned to β-H on the thiophene rings closer to BT units in **6a**, disappeared and signals at $\delta = 6.67$ ppm as a doublet, which correlated to the other β-H on the same thiophene ring, now appeared as a singlet with a significant 1.3–1.4 ppm downfield shift in the ^{1}H NMR spectrum of **1a**. This change clearly indicates the formation of a larger aromatic planar π system after cyclization.[42] In addition, the symmetric structures of **1a–b** are evidenced by only four proton signals, which can be assigned to the resonance from protons on the aromatic skeleton.

The large 2D π-conjugated structure of **1a–b** favored highly ordered self-assembly through π–π interactions, as evidenced by concentration-dependent ^{1}H NMR spectra in $CDCl_3$ (Figure 2). All aromatic proton resonances shifted upfield when the concentration of **1a** in $CDCl_3$ increased from 6 to

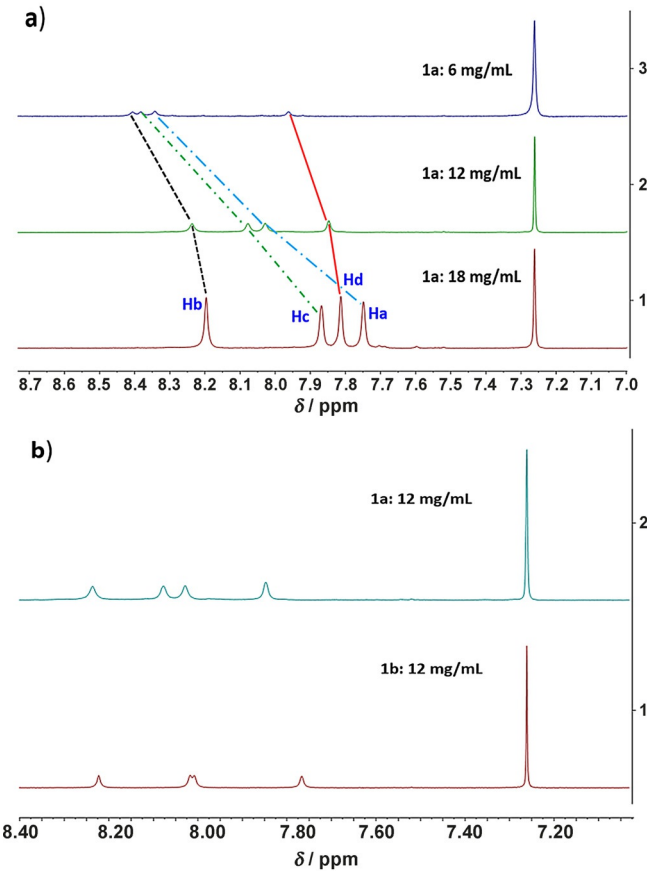

Figure 2. Aromatic region of the ^{1}H NMR spectra of a) **1a** in $CDCl_3$ at different concentrations; and b) **1a** and **1b** in $CDCl_3$ at the same concentration of 12 mg mL^{-1} (resonance assignments are shown in Figure 1).

18 mg mL^{-1} (Figure 2a). The two signals assigned to the protons of the DTNT units (Ha, Hb, and Hc) shifted upfield by approximately $\Delta\delta$Ha = 0.60 ppm, $\Delta\delta$Hb = 0.20 ppm, and $\Delta\delta$Hc = 0.50 ppm, when the concentration of **1a** in $CDCl_3$ increased from 6 to 18 mg mL^{-1}. A less pronounced upfield shift ($\Delta\delta$Hd = 0.10 ppm) was also observed for the protons in the NDT segment (Hd). Such upfield shifts were attributed to intermolecular shielding from the neighboring aromatic molecules in concentrated solution; this implied their tendency to self-associate through π–π interactions between neighboring molecules.[42] The chemical shifts of the protons (Ha, Hb, and Hc) on DTNT are more sensitive to concentrations than that of Hd on NDT core; this suggests that compounds **1a–b** should be contorted aromatics.[43] In comparison with **1a**, compound **1b** has a slightly different ^{1}H NMR spectrum at a very similar concentration of 12 mg mL^{-1} (as shown in Figure 2b), which indicates that the alkyl chains on the NDT core also influence molecular interactions in concentrated solution.

Thermal Properties

The thermal stability and thermally induced phase-transition behavior are important for organic semiconductors applied in organic electronic devices. TGA and DSC measurements were conducted to investigate the stability and phase transition of compounds **1a–b**. As shown in Figure 3a and b, both **1a** and **1b** exhibited good thermal stabilities, losing less than 5% weight upon being heated to 390 °C in nitrogen, as determined by TGA. Compound **1a**, with 3,7-dimethyloxyl chains, shows endothermal peaks at 298.7 °C and an exothermal peak at 267.5 °C (Figure 4a). This phenomenon suggests that compound **1a** is a crystalline material. However, no clear phase transition was observed when **1b** underwent several heating and cooling cycles under the same conditions (Figure 4b).

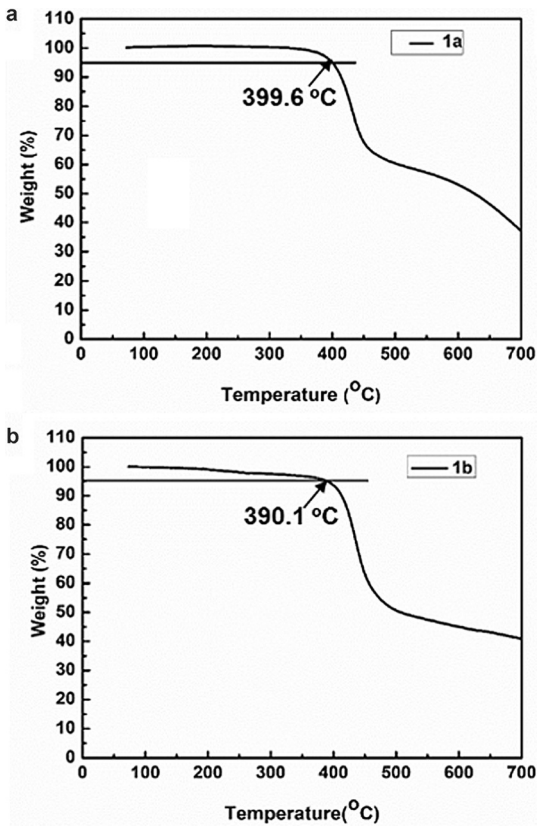

Figure 3. TGA curves of **1a** (a) and **1b** (b). The measurements were performed under a nitrogen atmosphere with heating and cooling rates of 10 °C min^{-1}.

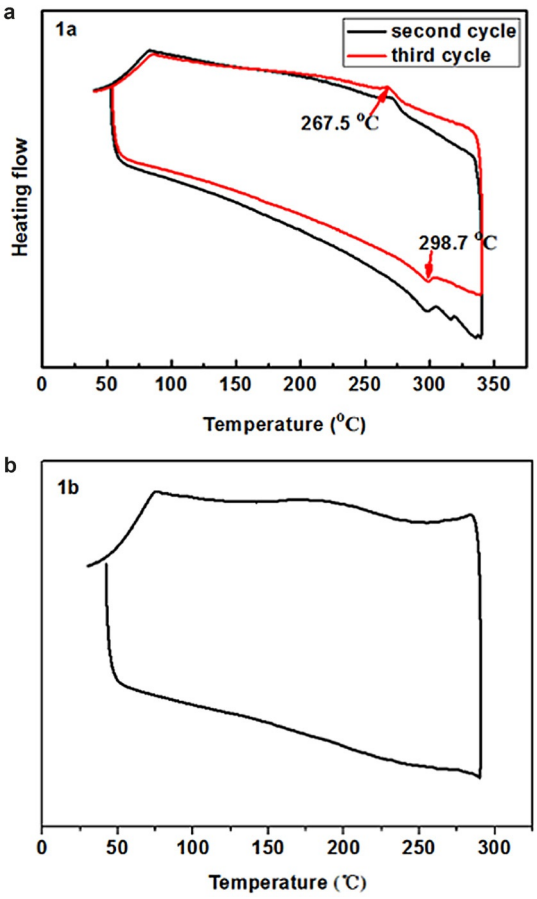

Figure 4. DSC curves of **1a** (a) and **1b** (b). The measurements were performed under a nitrogen atmosphere with heating and cooling rates of 10 °C min^{-1}.

XRD measurements were carried out on spin-coated films of **1a–b** to gain a good understanding of molecular packing and solid-state morphology. The pristine films were spin-coated on Si/SiO_2 substrates from a solution in chloroform (9 mg mL^{-1}). As shown in Figure 5, for compound **1b**, only a first-order reflection peak at around $2\theta = 5.88°$ with very strong intensity and a broad halo in the wide-angle region were observed. The XRD pattern of the spin-coated film of **1a** showed several reflection peaks. The reflections at $2\theta = 5.88$ and 10.47°, corresponding to *d* spacings of 15.12 and 8.44 Å, indicate long-range order, possibly with an edge-on molecular orientation. Considering disk-like 2D PAHs are likely to stack into similar columnar superstructures through intermolecular π–π interactions and other weak interactions in the solid state, com-

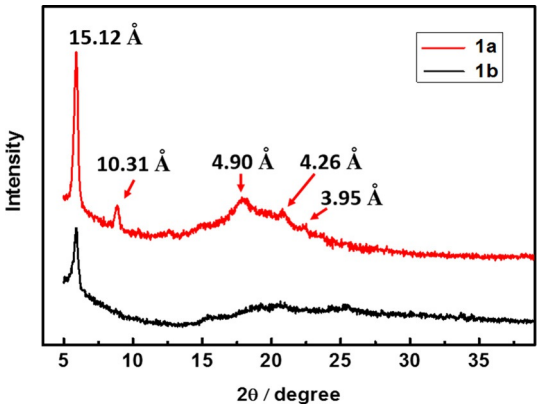

Figure 5. Thin-film XRD patterns of **1a–b**.

pounds **1a–b** should also adopt a columnar structure owing to strong π–π interactions between the largely extended rigid cores, although a very conclusive packing mode cannot be easily determined at the moment. Thus, the reflection peak at 3.95 Å can be correlated to the typical π–π stacking distance in each column. The peak at 4.26 Å can be correlated to the distance between the aliphatic chains by van der Waals interactions.[26a] Based on these results, we can conclude that with the same π system **1a** shows a better polycrystalline phase than **1b** because more sharp reflection peaks appeared in the XRD pattern of **1a** than **1b**. As shown in Figure 1, the only structural difference between **1a** and **1b** is their pendant alkyloxyl chains on the NDT center. The branched 3,4-dimethyloctyloxyl groups will increase the solubility of **1a**, which will allow more kinetically balanced aggregation in solution, leading to higher ordering packing in contrast to the faster aggregation of **1b**.[8] Thus, when precipitated from a concentrated solution or cast into a film, compound **1a** showed that a more ordered microphase should be reasonable. Finally, this will have an influence on their performances in FET devices.

Photophysical Properties

The UV/Vis absorption spectra of **1a–b** were recorded in dilute solutions (1×10^{-5} M) in chloroform and as thin films. The photoluminescence spectra of dilute solutions of **6a–b** and **1a–b** in chloroform were also recorded. For comparison, the absorption and emission spectra of **6a** were also recorded in $CHCl_3$ and as a film. All of the data are collected in Table 1and all spectra for **6a–b** and **1a–b** are included in Figure 6. The spectra for two pairs of compounds are almost identical to each other, respectively, so only representative spectra of **6a** and **1a** are shown in Figure 6. In solution, compound **6a** exhibits a strong π–π* transition with a maximum absorption at $\lambda\approx360$ nm and a strong charge-transfer band at $\lambda=424$ nm. For **1a**, its absorption spectrum exhibited three major bands with absorption $\lambda_{max}\approx312$, 389, and 451 nm. The absorption maximum of the charge-transfer band was redshifted by about 27 nm after ring closure, which indicated that **1a** had a lower band gap and more extended π-conjugation system.[23] The lowest energy absorption onsets of **6a** and **1a** in solution were at $\lambda=507$ and 575 nm, respectively, and the optical band gaps were calculated to be 2.44 and 2.15 eV for **6a** and **1a**, respectively. Vibronic bands for the absorption bands of **1a** were observed; these arose from enhanced rigidity in its chemical structure when formed from the cyclization of **6a**. Interestingly, in dilute solution **1a** shows similar absorption characteristics to that in DTNT.[34] For example, all absorption bands of DTNT, two absorption maxima in the UV region at $\lambda=368$ and 386 nm and one weak broad absorption band in the visible region at $\lambda=449$ nm, were observed in the absorption spectrum of **1a**, but with a slight redshift (<15 nm). This unexpected lower redshift in π–π* transition absorption band and intramolecular charge transition (ICT) band indicates that the fusion of two DTNT moieties onto the naphthalene core leads to a larger extended π system, but with constrained π-electron delocalization. Results of a Gaussian simulation on this point is discussed in the next section. In dilute solution, compounds **6a–b** and **1a–b** showed weak fluorescence at $\lambda_{em}=564.5$ (for **6a–b**) and 617.5 nm (for **1a–b**, as shown in Figure 7). After the

Table 1. Summary of the photophysical properties and electrochemical data for compounds **6a**, **6b**, **1a**, and **1b**.

	λ_{ab}	λ_{em}	E^{ox}_{onset}	E^{red}_{onset}	HOMO[a]	LUMO[a]	E_g^{opt}[b]	E_g^{ec}[a]
6a								
in solution[c]	343, 424	564.5	1.15	−0.70	−5.58	−3.73	2.44 (507)	1.85
in film[d]	347, 441							
6b								
in solution[c]	343, 425	564.5	1.13	−0.71	−5.56	−3.72	2.43 (509)	1.84
in film[d]	347, 463							
1a								
in solution[c]	315, 359, 389, 454	617.5	1.06	−0.69	−5.49	−3.74	2.15 (575)	1.75
in film[d]	381, 474, 576							
1b								
in solution[c]	314, 358, 388, 453	617.5	1.05	−0.70	−5.48	−3.73	2.15 (577)	1.75
in film[d]	389,469							

[a] HOMO/LUMO levels were calculated according to the following equations: HOMO $=-(E^{ox}_{onset}-E^{ferrocene}_{onset}+4.8)$ eV and LUMO $=-(E^{ox}_{onset}-E^{ferrocene}_{onset}+4.8)$ eV. E_g^{ec} of each compound was calculated from the empirical equation $E_g^{ec}=|E_{HOMO}-E_{LUMO}|$ eV. [b] Band gap estimated from the onset wavelength (λ_{onset}) of the solution optical absorption: $E_g^{opt}=1240/\lambda_{onset}$ eV. [c] Data recorded from solutions in chloroform (1×10^{-6} M). [d] Data recorded from thin films.

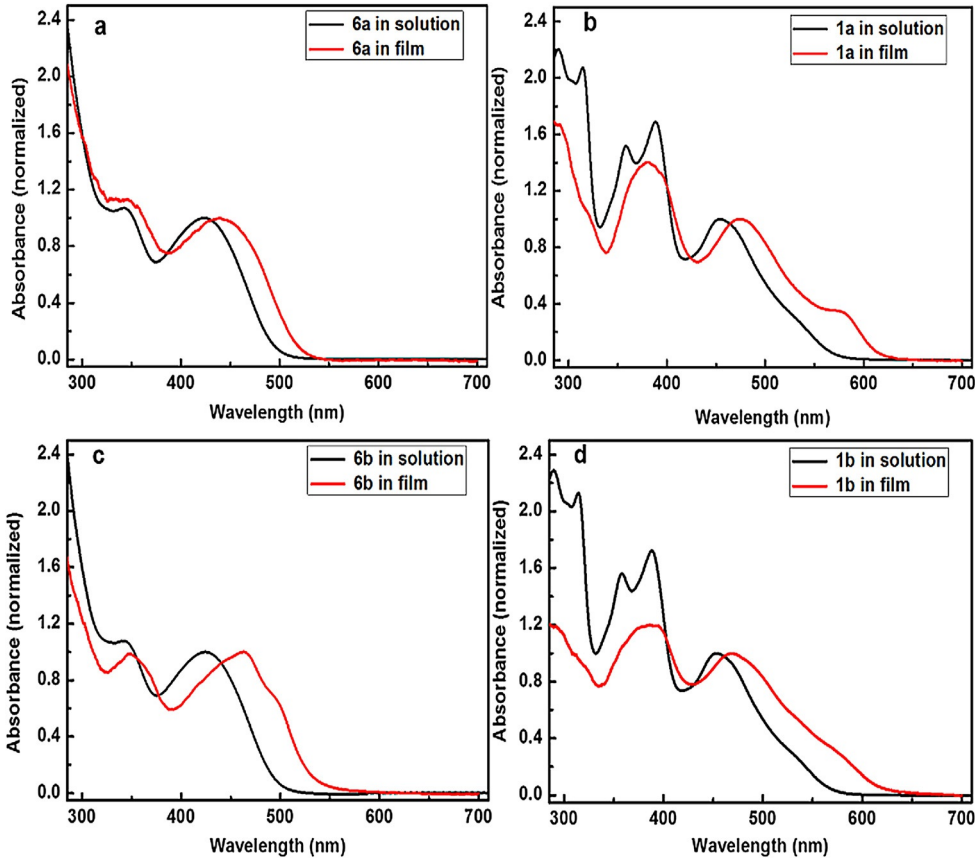

Figure 6. Normalized UV/Vis absorption spectra of **6a** (a), **1a** (b), **6b** (c), and **1b** (d) in chloroform (1.0×10^{-5} M) and in thin film (spin-coating from a solution in chloroform with a concentration of 9 mg mL^{-1}).

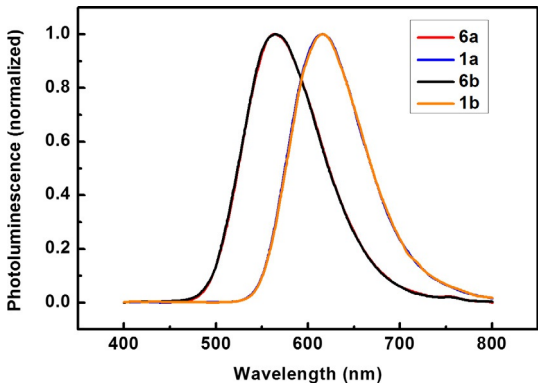

Figure 7. Normalized photoluminescence spectra of **6a** (red), **1a** (blue), **6b** (black), and **1b** (orange) as dilute solutions in chloroform (1.0×10^{-6} M).

ring-fusion step, the emission maxima redshifted by 53 nm, which indicated the formation of a larger π system. For both **6a** and **1a**, the UV/Vis absorption spectra as thin films were redshifted and broader than those in dilute solutions, which indicated that there was improved solid-state packing. Additionally, the absorption spectra of films were not vibronic owing to aggregation-induced intermolecular frontier orbital hybridization. In comparison with **1b**, the absorption spectrum of **1a** in a thin film shows a stronger shoulder at $\lambda = 576$ nm, which indicates that there are more ordered domains formed by π–π stacking when **1a** is aggregated in the film (as shown in Figure 6b and d).[44] This result agreed well with the results obtained by XRD measurements that in the film state **1a** showed more ordered packing than that of **1b**. With respect to intermolecular interactions in thick solutions shown by ^{1}H NMR spectroscopy, this kind of crystalline phase shown in the film state is reasonable. All of these results imply that even **1a**–**b** are in contorted butterfly-shaped architectures, which readily form ordered microstructures in solid films.

To further understand the electron density distribution and fundamentals of the molecular architecture of **1a**–**b**, DFT calculations were carried out by using the Gaussian 09 program.[37] To simplify the calculations, the parent skeleton with all alkyl side chains replaced by methyl groups was subjected to calculations (Figure 8c). The widely used Becke three-parameter hybrid functional combined with Becke–Lee–Yang–Parr correlation functional (B3LYP) using 6-31G(d) basis sets was employed to obtain a theoretical prediction of single molecular geometries and frontier orbital energy levels of the molecules at the ground states (S_0). The molecular electrostatic potential (ESP) was generated by using Gaussview 5.0, in which the red color describes a negative ESP and the blue represents positive ESP. The mean planes of aromatic moieties within **1a** were calculated based on the optimized structure obtained by DFT calculations with Diamond software. The calculated molecular struc-

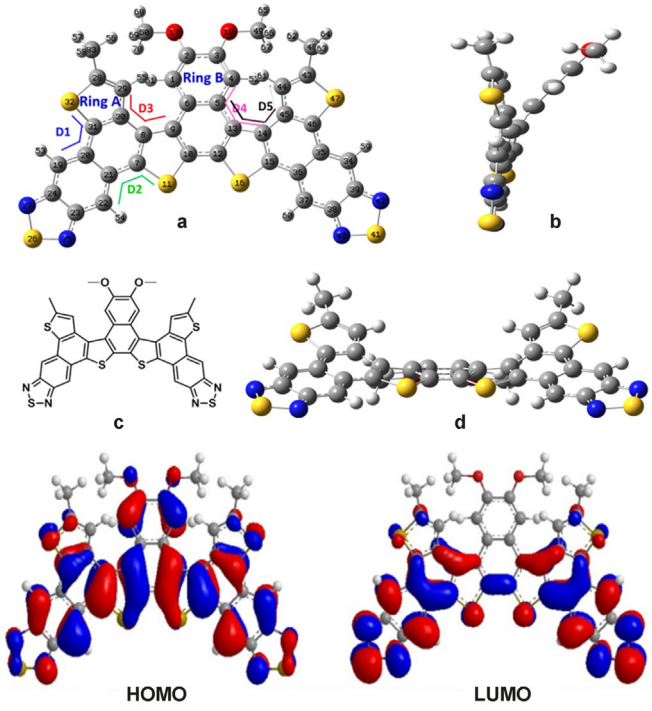

Figure 8. Calculated molecular structures (a–d) and frontier molecular orbital (FMO) profiles for **1a**–**b** (Rings A and B are set to calculate the mean plane angle (a), side view (b), model molecule (c), and front view (d)).

tures and FMO profiles of **1a** are shown in Figure 8. As predicted by calculations, compound **1a** shows a butterfly shape with highly contorted π conjugation, in which the naphthalene core and DTNT moieties are distorted in opposite directions. As shown in Figure 8a, b, and d, Ring A and Ring B are tilted with respect to each other by an angle of 44.8°, which is calculated based on the mean planes defined within the optimized molecular geometry. The dihedral angles of D1 and D2 (Figure 8a) are +9.9° and −6.7°, respectively; these values indicate that the DTNT moieties in compound **1a** are also twisted. The dihedral angles of D3, D4, and D5 are −11.1°, −16.9°, and −24.3°, respectively, which indicates that the NDT segment is also nonplanar. The highly distorted architecture of **1a** is presumably caused by ring constraint generated by fusion of the five-membered thiophene rings with the six-membered benzene ring to form a fused structure and large steric hindrance between the thiophene units on the DTNT units and the central naphthalene unit according to the calculated bond lengths. The strain in the molecular subunits severely distorts the aromatic molecules away from planarity, which results in limited π-electron delocalization along the whole molecular skeleton. The calculated HOMO and LUMO energy levels are −5.50 and −3.04 eV, respectively (Figure S24b in the Supporting Information), corresponding to a band gap of 2.46 eV. The calculated band gap is very close to the optical band gaps (Table 1). Compound **1a** adopts a partially disjoint FMO profile, that is, spatially separated HOMO and LUMO. The HOMO level resides along the thiophene moieties and naphthalene moiety, whereas the LUMO level is mainly localized on the electron-deficient DTNT moieties. Organic chromophores with a disjoint FMO structure always exhibit a limited ICT; thus energy transfer from the electron-donor part to the electron-deficient part is restricted. Theoretical calculation results reasonably support compounds **1a**–**b** showing similar absorption behavior to that of DTNT, although they were composed of by two fused DTNT units and one naphthalene unit. The term contorted aromatics is used to describe PAHs such as compounds **1a**–**b**,[45] which possess a large π-conjugated system, but constrained molecular structures. By using such PAHs, it can be expected that the curved π surfaces are useful as subunits to make self-assembled electronic materials.

Electrochemical Properties

For organic semiconducting materials in which charge transport occurs predominantly by hopping through their HOMOs and LUMOs, the relative energy levels are crucial in determining the injection of holes and electrons from the electrodes to the active layers, and consequently, affecting their performance in OFET devices.[4] The electrochemical properties of **1a**–**b** were examined by CV in dry dichloromethane. For comparison, CV measurements on **6a** and **6b** were also performed. The measured potentials were calibrated to the ferrocene/ferrocenium (Fc/Fc^+) couple. The HOMO and LUMO levels of these compounds were calculated from the onset oxidation (E^{ox}_{onset}) and reduction potentials (E^{red}_{onset}), respectively.[46] The CV profiles for **1a** and **1b** (**6a** and **6b**) are almost identical to each other (Figure 9 and Table 1), so only the profiles of **6a** and **1a** are discussed. Compound **6a** exhibited two partially reversible oxidation waves and two reversible reduction processes. The oxidation and reduction onsets of **6a** are estimated to be 1.15 and −0.70 V, respectively, which correspond to HOMO and LUMO levels of −5.58 and −3.73 eV, respectively. In contrast to **6a**, compound **1a** shows one quasi-reversible oxidation wave with E^{ox}_{onset} at 1.06 V and one reversible reduction wave with E^{red}_{onset} at −0.69 V, that is, the first oxidation potential is negatively shifted by 0.09 V, whereas the reduction potential is almost identical. According to differences in the onset potentials of oxidation and reduction, the electrochemical energy gaps of **6a** and **1a** are calculated to be 1.85 and 1.75 eV, respectively; this indicates that the band gaps become narrower when C–C bonds are formed within **6a** to afford a more delocalized π-conjugated system of **1a**. This is in good agreement with the trend of their optical band gaps. The corresponding HOMO level of **1a** is in excellent agreement with that predicted by DFT simulations, but the LUMO level of **1a** is about 0.7 eV lower than that of the DFT-derived value. The latter is mainly attributed to the lower accuracy of DFT in predicting the LUMO energies.[47] The HOMO level of **1a** shows a slight increase with the large π-extended conjugated system formed, whereas the LUMO levels are almost unaffected. This feature can be ascribed to the disjointed FMO profile, which permits the independent tuning of the HOMO and LUMO levels of the highly distorted butterfly-shaped PAHs. Therefore, the CV data are also in good agreement with the results obtained by UV/Vis absorption measurements and theoretical calculations. Fur-

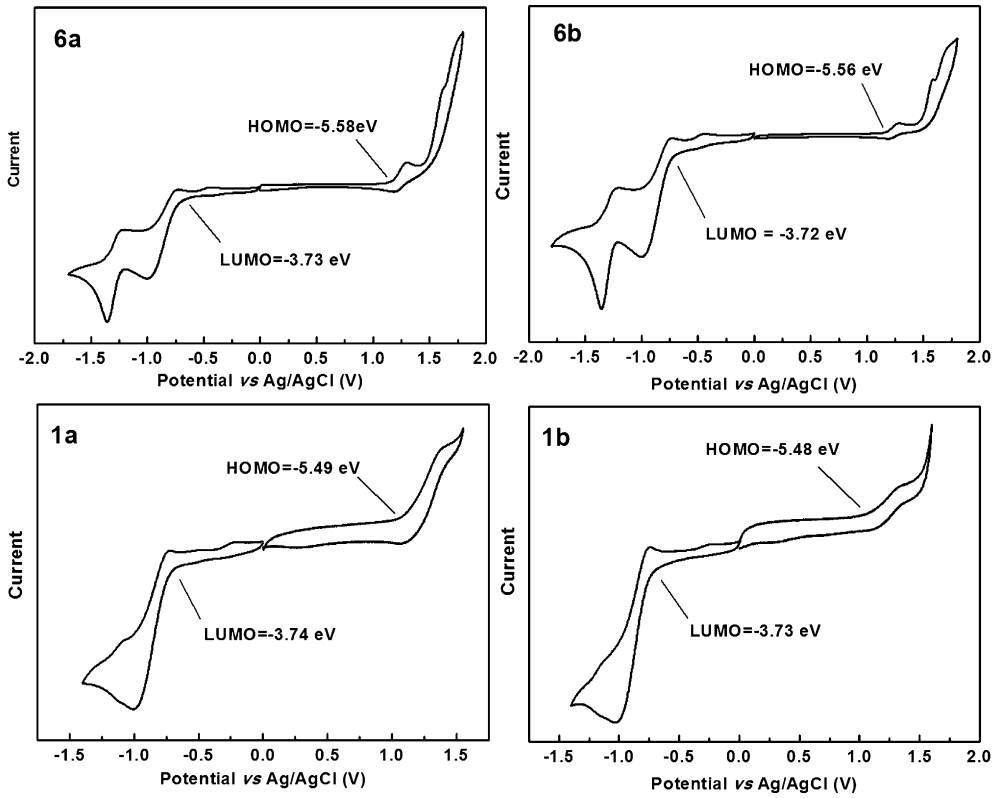

Figure 9. Cyclic voltammograms of compounds **6a**, **6b**, **1a**, and **1b** in dry CH_2Cl_2 with 0.1 M Bu_4NPF_6 as a supporting electrolyte. The scan rate was 50 mV s^{-1}.

thermore, both **6a** and **1a** possess good air stabilities owing to their HOMO energy level being lower than the air oxidation threshold of −5.27 eV.[48]

Fabrication and Characterization of FET Devices

Because compounds **1a**–**b** possess highly distorted molecular conformations and large delocalized π systems, it is necessary to examine their performance as organic semiconductors. OFET devices based on **1a**–**b** were fabricated by spin-coating solutions of the compounds in chloroform onto an octadecyltrichlorosilane (OTS)-modified SiO_2/Si substrate with a top-contact bottom-gate configuration.[49] Gold was used as the drain and source electrodes. Different annealing temperatures were screened to optimize the fabrication conditions. Although two DTNT moieties with ambipolar characteristics were fused into 12-ring heteroacenes of **1a**–**b**, transistors based on them exhibited typical p-channel transistor characteristics in air. The as-spun (unannealed) thin-film devices based on **1a** show a relatively low hole mobility of 1.34×10^{-3} $cm^2V^{-1}s^{-1}$ with a threshold voltage, V_{th}, of 18.3 V and a current on/off ratio of 2.83×10^3. After annealing the thin films at 160 °C for 5 min, the device showed an enhanced mobility of 3.27×10^{-2} $cm^2V^{-1}s^{-1}$, $V_{th}=6.98$ V, and current on/off ratio of 8.65×10^5. Typical output and transfer curves of the **1a**-based FET devices annealed at 160 °C are depicted in Figure 10. However, higher annealing temperatures resulted in decreased device performance (Table 2). The effect of thermal annealing on devices based on **1b** was different. When subjected to annealing temperatures ranging from 25 to 200 °C, the hole mobility of **1b**-based FET devices showed a stepwise improvement (Table 2). Although unclear, we speculate that such an improvement in device performance could be attributed to morphological changes to the active layer by higher temperature annealing. In comparison, the mobility of **1b**-based devices is one order of magnitude lower than that of the **1a**-based devices under optimized fabrication conditions. Notably, highly ordered semiconductors are expected to afford high hole mobilities.[3] As depicted in Figure 5, the thin film of **1a** shows stronger and more reflection peaks than that of **1b**, which clearly indicates that **1a** possesses more ordered packing in solution-processed thin films than **1b**. Thus, the relatively better device performances of the **1a**-based FETs are in good agreement with the thin-film XRD results. Although the mobility of compound **1a** was somewhat lower than those of linear acenes, the value was still among the highest values obtained for solution-processed FET devices fabricated with 2D PAHs. It was also expected that FET devices fabricated by utilizing microwires prepared with **1a** or **1b** could exhibit higher mobility, according to reports that organic microwire transistors could always exhibit mobility some orders of magnitude higher than those of their solution-processed devices.[31] A typical SEM image of microwires of **1a** is shown in Figure S28 in the Supporting Information.

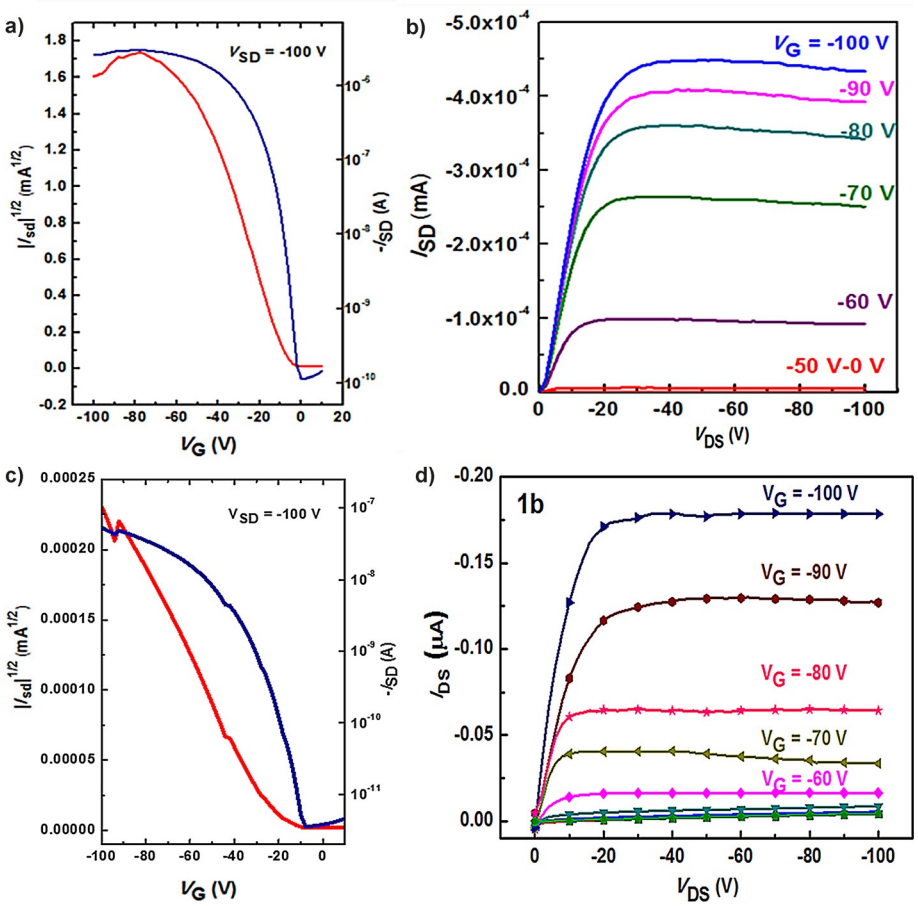

Figure 10. Typical transfer (a) and output (b) characteristics of the thin-film OFET based on **1a**. Typical transfer (c) and output (d) characteristics of the thin-film OFET based on **1b**. (Top-contact bottom-gate geometry, solution-processed onto OTS-modified Si/SiO_2 as solutions of 9 mg mL^{-1} in chloroform.)

Table 2. FET performance of **1a** and **1b** fabricated through a solution-processed method and treated with different thermal annealing temperatures. Average mobility values are obtained from six devices.

Material	T [°C]	μ_{ave} [cm^{2}V^{-1}s^{-1}]	μ_{max} [cm^{2}V^{-1}s^{-1}]	V_{th} [V]	I_{on}/I_{off} ratio
1a	25	1.23×10^{-3}	1.34×10^{-3}	18.3	2.83×10^{3}
	160	3.27×10^{-2}	3.54×10^{-2}	6.98	8.65×10^{5}
	180	1.96×10^{-2}	2.54×10^{-2}	13.9	2.67×10^{4}
	200	3.53×10^{-3}	4.67×10^{-3}	26.5	8.45×10^{4}
1b	25	1.18×10^{-5}	1.27×10^{-5}	18.0	5.24×10^{2}
	160	2.14×10^{-5}	2.46×10^{-5}	38.5	1.01×10^{3}
	180	6.53×10^{-5}	7.44×10^{-5}	18.8	4.63×10^{3}
	200	1.95×10^{-4}	3.02×10^{-4}	24.6	1.38×10^{4}

Conclusion

A new family of 1,2,5-thiadiazole-fused heteroacenes, featuring different alkyloxy substitution on the naphthalene center, were designed and synthesized by taking advantage of the Scholl annulation protocol. Both **1a** and **1b** were soluble in organic solvents, which implied superiority for solution processes. Optical, thermal, and electrochemical properties were investigated by UV/Vis absorption spectra, TGA, DSC, and CV measurements. Although DFT calculations showed that the molecular conformation was highly contorted, both concentration-dependent ^{1}H NMR spectra and thin-film XRD patterns showed their high tendency to self-associate through π–π interactions. To investigate the thin-film field-effect properties of these materials, a bottom-gate top-contact device configuration was adopted and the FET devices were fabricated by a solution-processed method. Preliminarily, OFETs based on **1a** exhibited p-channel characteristics with a mobility of up to 3.54×10^{-2} cm^{2}V^{-1}s^{-1}, a V_{th} value of 6.98 V, and an I_{on}/I_{off} ratio of 8.65×10^5 after optimized thermal annealing (Table 2). This performance is moderate but very impressive for highly contorted aromatics.[22,23] The mobility obtained from the device based on **1a** is among the highest mobility value obtained for solution-processed FETs based on 2D PAHs. This work provides a feasible strategy for a novel family of thiadiazole-fused 2D PAHs for solution-processed FET devices and reports useful insights into highly contorted aromatics for organic electronics. Further exploration of **1a**-based FETs is still warranted for higher FET mobility by fabricating microwire transistors.

Experimental Section

General Measurements and Characterization

All reagents were purchased from Sigma–Aldrich, Energy Chemical, J&K, and Suna Tech Inc. (P.R. China). They were used as received unless otherwise specified. Anhydrous toluene and THF were freshly distilled after being processed with sodium and benzophenone under an argon atmosphere prior to use. Other solvents and reagents were directly used without further treatment. 5,6-Dibromobenzo[*c*]-1,2,5-thiadiazole,[39] 3-(tri-*n*-butylstannyl)thiophene and 2-dodecylthiophene were synthesized by following literature procedures with optimization.[42] ^{1}H and ^{13}C NMR data were measured by using a Bruker Ultra Shield Plus AV400 spectrometer in deuterated chloroform at 298 K with tetramethylsilane (TMS; $\delta = 0$ ppm) as the internal standard (^{1}H NMR: 400 MHz, ^{13}C NMR: 100 MHz). GC-MS was recorded by using a Shimadazu GCMS-QP2010 plus instrument. MALDI-TOF MS was recorded by using a Bruker Autoflex II mass spectrometer with anthracene-1,8,9-triol as the matrix. Elemental analysis was performed on a Vario EL III Elementar system (Elementar Analyzen-systeme, Hanau, Germany). Elemental analyses were the average of three runs. All samples were measured simultaneously for C, H, N, and S. DSC analysis and TGA were performed on a Mettler DSC823e thermal analyzer and a Rigaku TG-DTA 8120 thermal analyzer, respectively, with a heating rate of 10 °C min^{-1} under a flow of nitrogen. UV/Vis absorption and fluorescence spectra were collected with a Shimadzu UV-1700 spectrometer and a RF-5301 fluorometer, respectively. Cyclic voltammograms were recorded in 0.1 M Bu_4NPF_6 in dry CH_2Cl_2 with a CHI 620C electrochemical analyzer. A gold disc with a diameter of 2 mm, a Pt wire, and an Ag/AgCl electrode were used as the working electrode, counter electrode, and reference electrode, respectively. The scan rate was 50.0 mV s^{-1}. For all CV measurements, Fc/Fc$^+$ redox couple was used as an internal standard, the oxidation potential of which ($E^{ferrocene}_{onset}$) was 0.37 V under the present test conditions. The HOMO energy levels were obtained from the equation HOMO $= -(E^{ox}_{onset} - E^{ferrocene}_{onset} + 4.8)$ eV. The LUMO levels of the polymer were obtained from the equation LUMO $= -(E^{red}_{onset} - E^{ferrocene}_{onset} + 4.8)$ eV. Room-temperature XRD measurements were performed on a Bruker-AXS D8 DISCOVER instrument with a GADDS powder X-ray diffractometer with $Cu_{K\alpha}$ radiation. The data were collected by using a Ni-filtered Cu-target tube at room temperature in the 2θ range from 5 to 40° at an angular rate of 0.2 s per step, with a scan step width of 0.02°. Field-emission SEM images were obtained by a field-emission scanning electron microscope (HITACHI S-4800).

Synthesis of 2a

In a 50 mL Schlenk tube, 4,5-dibromo-1,2-bis(dodecyloxy)benzene (2.75 g, 5 mmol) and 3-tributylstannylthiophene (4.66 g, 12.5 mmol) were mixed in freshly distilled toluene (20 mL). After carefully degassing with argon, [Pd(PPh$_3$)$_4$] (46 mg, 0.4 mmol) was added quickly under argon. The mixture was heated at 110 °C with stirring for 12 h in the dark. The cooled mixture was directly subjected to a vacuum evaporator to remove the solvent. The residue was further purified by column chromatography (silica gel, CH_2Cl_2/petroleum ether (PE) = 1/4, v/v) to give compound **2a** as a colorless oil (2.49 g, 90%). ^{1}H NMR (400 MHz, $CDCl_3$): $\delta = 7.17$ (dd, 2H), 7.02 (dd, 2H), 6.96 (s, 2H), 6.78 (dd, 2H), 4.13–4.01 (m, 4H), 1.90 (t, 2H), 1.66 (m, 2H), 1.57–1.47 (m, 2H), 1.38–1.09 (m, 14H), 0.99–0.93 (m, 6H), 0.86 ppm (t, 12H); ^{13}C NMR (100 MHz, $CDCl_3$): $\delta = 148.4$, 142.1, 129.2, 128.0, 124.6, 122.3, 115.6, 67.8, 39.3, 37.4, 36.3, 30.0, 28.1, 24.8, 22.8, 22.7, 19.8 ppm; GC-MS: *m/z* calcd for $C_{34}H_{50}O_2S_2$: 554.8896 (MW), 554.3252 (exact mass); found: 554.1.

Synthesis of 2b

Compound **2b** was obtained according to a similar procedure to that for **2a**. Pure **2b** was obtained as a waxy solid in good yield (92%). ^{1}H NMR (400 MHz, $CDCl_3$): $\delta = 7.17$ (dd, 2H), 7.01 (dd, 2H), 6.95 (s, 2H), 6.77 (dd, 2H), 4.04 (m, 4H), 1.89–1.78 (m, 4H), 1.52–1.44 (m, 4H), 1.26 (s, 32H), 0.95 (d, 6H), 0.86 ppm (t, $J = 6.8$ Hz, 12H); ^{13}C NMR (100 MHz, $CDCl_3$): $\delta = 148.4$, 142.1, 129.1, 128.0, 124.5, 122.3, 115.7, 69.5, 32.0, 29.7, 29.70, 29.68, 29.68, 29.5, 29.41, 29.35, 26.1, 22.7, 14.2 ppm; MALDI-TOF MS: *m/z* calcd for $C_{38}H_{58}O_2S_2$: 610.9959 (MW), 610.3878 (exact mass); found: 609.994.

Synthesis of 3a

A solution of **2a** (112 mg, 0.2 mmol) in dry CH_2Cl_2 (50 mL) was degassed by bubbling through nitrogen gas for 15 min. $FeCl_3$ (65 mg, 0.4 mmol) in anhydrous CH_3NO_2 (0.6 mL) was then added dropwise by means of a syringe over the course of 10 min. The dark-green solution was kept stirring and bubbling with a flow of nitrogen for 15 min and then the reaction was quenched with methanol (60 mL). The mixture was extracted with CH_2Cl_2 and the combined organic phase was dried over Na_2SO_4. The solvent was removed under vacuum and the residue was purified by column chromatography (silica gel, hexane/CH_2Cl_2 = 2/1, v/v) to give **3a** as a white solid (89 mg, 80%). ^{1}H NMR (400 MHz, $CDCl_3$): $\delta = 7.88$ (d, 2H), 7.70 (s, 2H), 7.48 (d, 2H), 4.31–4.17 (m, 4H), 2.05–1.94 (m, 2H), 1.82–1.67 (m, 4H), 1.60–1.49 (m, 2H), 1.45–1.29 (m, 6H), 1.24–1.14 (m, 6H), 1.02 ppm (d, 6H), 0.88 (d, $J = 6.6$ Hz, 12H); ^{13}C NMR (100 MHz, $CDCl_3$): $\delta = 148.8$, 133.9, 130.4, 123.4, 122.7, 122.6, 106.6, 67.6, 39.4, 37.6, 36.3, 30.1, 28.1, 24.9, 22.9, 22.8, 19.9 ppm; MALDI-TOF MS: *m/z* calcd for $C_{34}H_{48}O_2S_2$: calcd 552.8737 (MW), 552.3096 (exact mass); found: 551.860.

Synthesis of 3b

Compound **3b** was synthesized by following the same procedure as that used for **3a** to give **3b** as a white solid (75%). ^{1}H NMR (400 MHz, $CDCl_3$): $\delta = 7.88$ (d, 2H), 7.70 (s, 2H), 7.47 (d, 2H), 4.20 (t, 4H), 1.99–1.89 (m, 4H), 1.55 (t, 4H), 1.27 (s, 32H), 0.88 ppm (t, 6H); ^{13}C NMR (100 MHz, $CDCl_3$): $\delta = 148.9$, 133.9, 130.4, 123.4, 122.8, 122.6, 106.8, 69.3, 32.0, 29.8, 29.7, 29.5, 29.4, 29.3, 26.2, 22.8, 14.2 ppm; MALDI-TOF MS: *m/z* calcd for $C_{38}H_{56}O_2S_2$: 608.9800 (MW), 608.3722 (exact mass); found: 607.987.

Synthesis of 4a

*n*BuLi (2.6 mL, 4.1 mmol, 1.6 M in hexanes) was added by means of a syringe under argon to a solution of compound **3a** (1.10 g, 2 mmol) in dry THF (15 mL) at −78 °C. The mixture was kept stirring at −78 °C for 2 h before tributyltin chloride (1.32 mL, 4.4 mmol) was added. The reaction mixture was then kept at room temperature for another 8 h. The mixture was extracted with PE (2 × 30 mL) and the combined organic phase was dried over Na_2SO_4. The solvent was removed under vacuum to give compound **4a** quantitatively as a yellow liquid (2.38 g). Compound **4a** was used without further purification. ^{1}H NMR (400 MHz, $CDCl_3$): $\delta = 7.86$ (s, 2H), 7.75 (s, 2H), 4.28 (t, 4H), 2.02 (m, 2H), 1.70–1.51 (m, 12H), 1.46–1.19 (m, 58H), 1.13–1.08 (m, 8H), 0.95–0.83 ppm (m, 61H). (Inexact integration was caused by the excess use of tributylstannyl chloride, but the integration and resonance signals down-

field and at $\delta = 4.25$ and 2.02 ppm could help us to confirm the quality of **4a**.)

Synthesis of 4b

Compound **4b** was prepared according to the same procedure as that used for **4a** to give **4b** as a yellow liquid (95%). ^{1}H NMR (400 MHz, $CDCl_3$): $\delta = 7.86$ (s, 2H), 7.75 (s, 2H), 4.23 (m, 4H), 1.95 (m, 4H), 1.69–1.60 (br, 45H), 1.39 (br, 7.3 Hz, 153H), 1.24–1.02 (m, 9.2 Hz, 12H), 0.98–0.83 ppm (m, 100H).

Synthesis of 5

In a 50 mL Schlenk tube, 5,6-dibromobenzo[*b*]-2,1,3-thiadiazole (2.94 g, 10 mmol), 2-dodecylthiophene (2.77 g, 11 mmol), anhydrous K_2CO_3 (1.66 g, 12 mmol), and PivOH (306 mg, 3 mmol) were stirred in anhydrous DMA (20 mL) at 110 °C for 4 h under an argon atmosphere. After cooling to room temperature, the mixture was extracted with ethyl acetate (3×30 mL). The combined organic phase was dried over Na_2SO_4. The solvent was removed under vacuum, then **5** was purified by column chromatography (silica gel, CH_2Cl_2/PE = 1/8, v/v) as the eluent to give compound **5** as a yellow oil (3.40 g, 73%). ^{1}H NMR (400 MHz, $CDCl_3$): $\delta = 8.40$ (s, 1H), 8.08 (s, 1H), 7.19 (d, 1H), 6.82 (d, 1H), 2.87 (t, 2H), 1.74 (m, 2H), 1.26 (br, 18H), 0.88 ppm (t, 3H); ^{13}C NMR (100 MHz, $CDCl_3$): $\delta = 154.1$, 153.7, 148.4, 137.4, 137.0, 128.9, 126.4, 125.2, 124.3, 122.3, 31.9, 31.6, 30.2, 29.69, 29.66, 29.57, 29.4, 29.2, 22.7, 14.1 ppm; GC-MS: *m/z* calcd for $C_{22}H_{29}BrN_2S_2$: 465.5131 (MW), 464.0956 (exact mass); found: 465.9

Synthesis of 6a

In a 50 mL Schlenk tube, compounds **4a** (1.13 g, 1.0 mmol) and **5** (1.02 g, 2.2 mmol) were mixed in freshly distilled toluene (30 mL). After careful degassing with argon, [$Pd(PPh_3)_4$] (60 mg, 0.5 mmol) was added quickly under argon. The mixture was heated at 110 °C with stirring for 12 h in the dark. The cooled mixture was directly subjected to a vacuum evaporator to remove the solvent. The residue was further purified by column chromatography (silica gel, CH_2Cl_2/PE = 1/2, v/v) to give compound **6a** as an orange solid (925 mg, 70%). ^{1}H NMR (400 MHz, $CDCl_3$): $\delta = 8.28$ (s, 2H), 8.15 (s, 2H), 7.75 (s, 2H), 7.53 (s, 2H), 6.89 (d, 2H), 6.67 (d, 2H), 4.25–4.14 (m, 4H), 2.75 (t, 4H), 1.82–1.68 (m, 2H), 1.82–1.69 (m, 4H), 1.66–1.49 (m, 8H), 1.42–1.09 (m, 40H), 1.02 (d, $J = 6.4$ Hz, 6H), 0.90–0.83 ppm (m, 24H); ^{13}C NMR (100 MHz, $CDCl_3$): $\delta = 154.3$, 154.1, 149.0, 148.5, 139.7, 138.1, 136.7, 136.5, 134.2, 131.2, 128.4, 124.4, 123.6, 122.7, 122.6, 122.3, 106.4, 67.5, 39.3, 37.5, 36.2, 31.9, 31.7, 30.14, 30.11, 30.10, 29.72, 29.66, 29.65, 29.5, 29.4, 29.3, 29.0, 28.0, 24.8, 22.74, 22.70, 22.64, 19.8, 14.1 ppm; MALDI-TOF MS: *m/z* calcd for $C_{78}H_{104}N_4O_2S_6$: 1320.65; found: 1320.51; elemental analysis calcd (%) for $C_{78}H_{104}N_4O_2S_6$: C 70.86, H 7.93, N 4.24, S 14.55; found: C 70.88, H 7.90, N 4.23, S 14.53.

Synthesis of 6b

Compound **6b** was prepared according to the same procedure as that used for **6a** to give **6b** as an orange solid (63%). ^{1}H NMR (400 MHz, $CDCl_3$): $\delta = 8.27$ (s, 2H), 8.15 (s, 2H), 7.72 (s, 2H), 7.51 (s, 2H), 6.88 (d, 2H), 6.67 (d, 2H), 4.16 (t, 4H), 2.75 (t, 4H), 1.99–1.89 (m, 4H), 1.64–1.49 (m, 8H), 1.36–1.07 (m, 68H), 0.91–0.79 ppm (m, 12H); ^{13}C NMR (100 MHz, $CDCl_3$): $\delta = 154.3$, 154.1, 149.0, 148.4, 139.6, 138.0, 136.7, 136.4, 134.2, 131.2, 128.4, 124.4, 123.6, 122.7, 122.6, 122.4, 106.4, 69.2, 32.0, 31.9, 31.7, 30.1, 29.77, 29.73, 29.71, 29.67, 29.55, 29.51, 29.41, 29.38, 29.3, 29.0, 26.2, 22.7, 14.2, 14.1 ppm; MALDI-TOF MS: *m/z* calcd for $C_{82}H_{112}N_4O_2S_6$: 1376.71; found: 1376.56; elemental analysis calcd (%) for $C_{82}H_{112}N_4O_2S_6$: C 71.46, H 8.19, N 4.07, S 13.96; found: C 71.47, H 8.16, N 4.07, S 13.93.

Synthesis of 1a

A solution of **6a** (133 mg, 0.1 mmol) in dry CH_2Cl_2 (50 mL) was degassed by bubbling through nitrogen gas for 15 min. $FeCl_3$ (162 mg, 1.0 mmol) in anhydrous CH_3NO_2 (0.8 mL) was then added dropwise by means of a syringe over the course of 15 min. The dark-green solution was kept stirring and bubbling with a flow of nitrogen for another 30 min and then the reaction was quenched with methanol (60 mL). The precipitate was collected and washed with methanol before being dissolved in CH_2Cl_2 (50 mL). The solution was washed with brine for twice and dried over Na_2SO_4. The solvent was removed under vacuum and the residue was purified by column chromatography (silica gel, PE/CH_2Cl_2 = 1/1, v/v) to give **1a** as a red solid (86 mg, 65%). ^{1}H NMR (400 MHz, $CDCl_3$): $\delta = 8.20$ (s, 2H), 7.87 (s, 2H), 7.81 (s, 2H), 7.75 (s, 2H), 4.43 (s, 4H), 2.95–2.82 (t, 4H), 2.22–2.10 (m, 2H), 2.00–1.91 (m, 2H), 1.89–1.71 (m, 6H), 1.28–1.30 (m, 50H), 1.14 (d, 6H), 0.91 ppm (d, 18H); ^{13}C NMR (100 MHz, $CDCl_3$): $\delta = 152.2$, 151.8, 147.3, 146.3, 134.5, 134.4, 133.1, 131.3, 130.5, 129.3, 128.9, 128.2, 124.1, 124.0, 114.0, 112.9, 109.4, 67.6, 39.4, 37.9, 37.8, 32.0, 31.9, 31.2, 30.3, 29.83, 29.81, 29.75, 29.65, 29.4, 28.1, 25.0, 22.8, 22.74, 22.71, 22.70, 19.90, 19.86, 14.2 ppm; MALDI-TOF MS: *m/z* calcd for $C_{78}H_{100}N_4O_2S_6$: 1316.62; found: 1376.46; elemental analysis calcd (%) for $C_{78}H_{100}N_4O_2S_6$: C 71.08, H 7.65, N 4.25, S 14.60; found: C 71.11, H 7.65, N 4.26, S 14.58.

Synthesis of 1b

Compound **1b** was prepared according to the same procedure as that used for **1a**. Owing to strong π–π stacking interactions and relatively low solubility in CH_2Cl_2, compound **1b** can only be washed from the column of silica gel by chloroform. Pure **1b** was obtained by recrystallization from a mixture of chloroform and hexane as a red solid (60%). ^{1}H NMR (400 MHz, $CDCl_3$): $\delta = 8.22$ (s, 2H), 8.02 (s, 2H), 8.01 (s, 2H), 7.77 (s, 2H), 4.37 (t, 4H), 2.95–2.85 (t, 4H), 2.13–2.03 (m, 4H), 1.85–1.76 (m, 4H), 1.67–1.74 (m, 4H), 1.29 (s, 68H), 0.89 ppm (t, 12H). Although an unambiguous ^{1}H NMR spectrum of **1b** can be readily obtained, it is difficult to collect the ^{13}C NMR spectrum. However, by comparing the MALDI-TOF mass spectrum of **6b** and **1b**, it could be conclusively confirmed that **1b** was obtained by us. MALDI-TOF MS: *m/z* calcd for $C_{82}H_{108}N_4O_2S_6$: 1372.68; found: 1372.48; elemental analysis calcd for $C_{82}H_{108}N_4O_2S_6$: C 71.67, H 7.92, N 4.08, S 14.00; found: C 71.70, H 7.93, N 4.10, S 13.94.

Synthesis of 7b

Compound **7b** (55%) was obtained by following the same procedure as that used for **1a**, but with 4 equivalents of $FeCl_3$. ^{1}H NMR (400 MHz, $CDCl_3$): $\delta = 8.61$ (s, 1H), 8.59 (s, 1H), 8.30 (s, 1H), 8.14 (s, 1H), 8.13 (s, 1H), 7.87 (s, 1H), 7.67 (s, 1H), 7.48 (s, 1H), 6.91 (d, 2H), 6.69 (d, 2H), 4.43 (m, 4H), 2.95 (t, 2H), 2.76 (t, 2H), 2.02–1.92 (m, 4H), 1.80 (t, 2H), 1.58 ppm (m, 19H) (inexact integration at 1.26–0.8 ppm originated from overlap with the resonances of PE); MALDI-TOF MS: *m/z* calcd for $C_{82}H_{110}N_4O_2S_6$: 1374.70; found: 1374.50; elemental analysis calcd (%) for $C_{82}H_{110}N_4O_2S_6$: C 71.57, H 8.06, N 4.07, S 13.98; found: C 71.61, H 7.98, N 4.10, S 13.95.

OFET Device Fabrication and Characterization

Top-contact, bottom-gate FET devices were prepared according to methods reported by Bao et al.[49] A heavily p-doped silicon wafer with a 200 nm thermal SiO_2 layer was used as the substrate/gate electrode. The SiO_2/Si substrate was cleaned with acetone and isopropanol, then immersed in a piranha solution for 8 min. Followed by rinsing with deionized water, the wafer was cast with a 3 mM solution of OTS in trichloroethylene. Then it was placed in an environment saturated with ammonia vapor for 7 h at room temperature. The semiconductor layer was deposited on top of the OTS-modified dielectric surface by spin-coating the solution of **1a** or **1b** in chloroform (9 mg mL^{-1}) at 1500 rpm for 60 s. Then the thin films were annealed at various temperatures for 5 min under a nitrogen atmosphere. Subsequently, gold source/drain electrodes were deposited by thermal evaporation through a metal shadow mask to create a series of FETs with a channel length of $L = 100$ μm and a width of $W = 1$ mm. Characteristics of the OFET devices were measured at room temperature under ambient conditions by using a Keithley 4200 semiconducting parameter analyzer. Field-effect mobility was extracted in the saturation regime of I_D by using Equation (1) in the saturation regime from the gate sweep:

$$I_D = \frac{\mu W C_i}{2L}(V_g - V_T)^2 \quad (1)$$

in which I_D is the drain current; μ is the field-effect mobility; C_i is the capacitance per unit area of the gate dielectric layer (SiO_2, 200 nm, $C_i = 17.25$ nF cm^{-2}); V_G and V_T are the gate and threshold voltages, respectively; and W and L are the channel width and length, respectively. The current on/off ratio was determined from I_D at $V_G = 0$ V (I_{off}) and $V_G = -100$ V (I_{on}). The μ_{FET} data reported were typical values from six different devices.

Acknowledgements

B.M.Z. acknowledges financial support from the National Basic Research Program of China(2012CB933301), the National Natural Science Foundation of China (51103074, 51203077, 21204038, 81273409, 61474062, 61136003), the Natural Science Foundation of Jiangsu Province (BK2012438, BM2012010), the Sci-tech Support Planof Jiangsu Province (BE2014719), the Priority Academic Program Development of Jiangsu Higher Education Institutions (PAPD), the Program for Changjiang Scholars and Innovative Research Team in University (IRT-15R37), the Synergetic Innovation Center for Organic Electronics and Information Displays, and the Specialized Research Fund for the Doctoral Program of Higher Education(20113223110005).

Keywords: aromaticity · conjugation · fused-ring systems · polycyclic aromatic hydrocarbons · synthesis design

[1] J. E. Anthony, *Chem. Rev.* **2006**, *106*, 5028 – 5048.
[2] M. Muccini, *Nat. Mater.* **2006**, *5*, 605 – 613.
[3] J. G. Mei, Y. Diao, A. L. Appleton, L. Fang, Z. N. Bao, *J. Am. Chem. Soc.* **2013**, *135*, 6724 – 6746.
[4] C. Wang, H. L. Dong, W. P. Hu, Y. Q. Liu, D. B. Zhu, *Chem. Rev.* **2012**, *112*, 2208 – 2267.
[5] Q. Miao, *Adv. Mater.* **2014**, *26*, 5541 – 5549.
[6] J.-I. Park, J. W. Chung, J.-Y. Kim, J. J. Lee, J. Y. Jung, B. Koo, B.-L. Lee, S. W. Lee, Y. W. Jin, S. Y. Lee, *J. Am. Chem. Soc.* **2015**, *137*, 12175 – 12178.
[7] H. Minemawari, T. Yamada, H. Matsui, J. Y. Tsutsumi, S. Haas, R. Chiba, R. Kumai, T. Hasegawa, *Nature* **2011**, *475*, 364 – 367.
[8] Y. Yamashita, F. Hinkel, T. Marszalek, W. Zajaczkowski, W. Pisula, M. Baumgarten, H. Matsui, K. Müllen, J. Takeya, *Chem. Mater.* **2016**, *28*, 420 – 424.
[9] P. M. Beaujuge, J. M. J. Fréchet, *J. Am. Chem. Soc.* **2011**, *133*, 20009 – 20029.
[10] Y. Wen, Y. Q. Liu, Y. L. Guo, G. Yu, W. P. Hu, *Chem. Rev.* **2011**, *111*, 3358 – 3406.
[11] H. L. Dong, X. L. Fu, J. Liu, Z. R. Wang, W. P. Hu, *Adv. Mater.* **2013**, 25, 6158 – 6183.
[12] M. Watanabe, K.-Y. Chen, Y. J. Chang, T. J. Chow, *Acc. Chem. Res.* **2013**, *46*, 1606 – 1615.
[13] Q. Ye, C. Y. Chi, *Chem. Mater.* **2014**, *26*, 4046 – 4056.
[14] U. H. F. Bunz, *Acc. Chem. Res.* **2015**, *48*, 1676 – 1686.
[15] J. S. Wu, W. Pisula, K. Müllen, *Chem. Rev.* **2007**, *107*, 718 – 747.
[16] a) K. Takimiya, I. Osaka, T. Mori, M. Nakano, *Acc. Chem. Res.* **2014**, *47*, 1493 – 1502; b) A. Fukazawa, S. Yamaguchi, *Chem. Asian J.* **2009**, *4*, 1386 – 1400.
[17] J. E. Anthony, *Angew. Chem. Int. Ed.* **2008**, *47*, 452 – 483; *Angew. Chem.* **2008**, *120*, 460 – 492.
[18] Y. Zhou, W. Liu, Y. Ma, H. Wang, L. Qi, Y. Cao, J. Y. Wang, J. Pei, *J. Am. Chem. Soc.* **2007**, *129*, 12386 – 12387.
[19] Q. F. Yan, Y. Zhou, B. B. Ni, Y. G. Ma, J. Y. Wang, J. Pei, Y. Cao, *J. Org. Chem.* **2008**, *73*, 5328 – 5339.
[20] W. F. Zhang, X. N. Sun, P. F. Xia, J. Y. Huang, G. Yu, M. S. Wong, Y. Q. Liu, D. B. Zhu, *Org. Lett.* **2012**, *14*, 4382 – 4385.
[21] Y. Zhou, T. Lei, L. Wang, J. Pei, Y. Cao, J. Wang, *Adv. Mater.* **2010**, *22*, 1484 – 1487.
[22] J. Yin, Y. Zhou, T. Lei, J. Pei, *Angew. Chem. Int. Ed.* **2011**, *50*, 6320 – 6323; *Angew. Chem.* **2011**, *123*, 6444 – 6447.
[23] W. Jiang, Y. Zhou, H. Geng, S. Jiang, S. Yan, W. Hu, Z. Wang, Z. G. Shuai, J. Pei, *J. Am. Chem. Soc.* **2011**, *133*, 1 – 3.
[24] L. Zhang, A. Fonari, Y. Liu, A. Hoyt, H. Lee, D. Granger, S. Parkin, T. P. Russell, J. E. Anthony, J. L. Brédas, V. Coropceanu, A. L. Briseno, *J. Am. Chem. Soc.* **2014**, *136*, 9248 – 9251.
[25] L. Chen, S. R. Puniredd, Y.-Z. Tan, M. Baumgarten, U. Zschieschang, V. Enkelmann, W. Pisula, X. L. Feng, H. Klauk, K. Müllen, *J. Am. Chem. Soc.* **2012**, *134*, 17869 – 17872.
[26] a) B. M. Zhao, B. Liu, R. Q. Png, K. Zhang, K. A. Lim, J. Luo, J. J. Shao, P. K. H. Ho, C. Y. Chi, J. S. Wu, *Chem. Mater.* **2010**, *22*, 435 – 449; b) L. Zöphel, D. Beckmann, V. Enkelmann, D. Chercka, R. Rieger, K. Müllen, *Chem. Commun.* **2011**, *47*, 6960 – 6962; c) D. Waghray, C. de Vet, K. Karypidou, W. Dehaen, *J. Org. Chem.* **2013**, *78*, 11147 – 11154; d) J. X. Zhang, T. C. Parker, W. Chen, L. Williams, V. N. Khrustalev, E. V. Jucov, S. Barlow, T. V. Timofeeva, S. R. Marder, *J. Org. Chem.* **2016**, *81*, 360 – 370.
[27] J. D. Tovar, T. M. Swager, *Adv. Mater.* **2001**, *13*, 1775 – 1780.
[28] J. D. Tovar, A. Rose, T. M. Swager, *J. Am. Chem. Soc.* **2002**, *124*, 7762 – 7769.
[29] C. J. Jiao, K.-W. Huang, Z. P. Guan, Q. H. Xu, J. S. Wu, *Org. Lett.* **2010**, *12*, 4046 – 4049.
[30] X.-Y. Wang, F.-D. Zhuang, R.-B. Wang, X.-C. Wang, X.-Y. Cao, J.-Y. Wang, J. Pei, *J. Am. Chem. Soc.* **2014**, *136*, 3764 – 3767.
[31] J. H. Dou, Y. Q. Zheng, Z. F. Yao, T. Lei, X. Sheng, X. Y. Luo, Z. A. Yu, S. D. Zhang, G. Han, Z. Wang, Y. P. Yi, J. Y. Wang, J. Pei, *Adv. Mater.* **2015**, *27*, 8051 – 8055.
[32] A. Facchetti, M. H. Yoon, C. L. Stern, G. R. Hutchison, M. A. Ratner, T. J. Marks, *J. Am. Chem. Soc.* **2004**, *126*, 13480 – 13501.
[33] a) H. M. Qu, W. B. Cui, J. L. Li, J. J. Shao, C. Y. Chi, *Org. Lett.* **2011**, *13*, 924 – 927; b) M. Nitani, Y. Ie, H. Tada, Y. Aso, *Chem. Asian J.* **2011**, *6*, 2352 – 2361; c) Y. H. Li, G. X. Zhang, W. Zhang, J. G. Wang, X. Chen, Z. T. Liu, Y. L. Yan, Y. S. Zhao, D. Q. Zhang, *Chem. Asian J.* **2014**, *9*, 3207 – 3214.
[34] A. L. Appleton, S. Miao, S. M. Brombosz, N. J. Berger, S. Barlow, S. R. Marder, B. M. Lawrence, K. I. Hardcastle, U. H. F. Bunz, *Org. Lett.* **2009**, *11*, 5222 – 5225.
[35] T. Lei, Y. Zhou, C.-Y. Cheng, Y. Cao, Y. Peng, J. Bian, J. Pei, *Org. Lett.* **2011**, *13*, 2642 – 2645.
[36] Q. Shuai, H. T. Black, A. Dadvand, D. F. Perepichka, *J. Mater. Chem. C* **2014**, *2*, 3972 – 3979.

[37] Z. F. Shi, H. T. Black, A. Dadvand, D. F. Perepichka, *J. Org. Chem.* **2014**, *79*, 5858 – 5860.
[38] D. Cortizo-Lacalle, C. Gozalvez, M. Olano, X. N. Sun, M. Melle-Franco, L. E. Hueso, A. Mateo-Alonso, *Org. Lett.* **2015**, *17*, 5902 – 5905.
[39] J. J. Shao, J. J. Chang, C. Y. Chi, *Org. Biomol. Chem.* **2012**, *10*, 7045 – 7052.
[40] H. Y. Huang, G. Y. Jiao, S. L. Liu, Q. Li, X. Shi, N. N. Fu, L. H. Wang, B. M. Zhao, W. Huang, *Chem. Commun.* **2015**, *51*, 15846 – 15849.
[41] L. G. Mercier, M. Leclerc, *Acc. Chem. Res.* **2013**, *46*, 1597 – 1605.
[42] J. Luo, B. M. Zhao, H. Z. O. Chan, C. Y. Chi, *J. Mater. Chem.* **2010**, *20*, 1932 – 1941.
[43] L. Zhang, Y. Cao, N. S. Colella, Y. Liang, J.-L. Bredas, K. N. Houk, A. L. Briseno, *Acc. Chem. Res.* **2015**, *48*, 500 – 509.
[44] Q. Ye, J. J. Chang, K.-W. Huang, C. Y. Chi, *Org. Lett.* **2011**, *13*, 5960 – 5963.
[45] M. Ball, Y. Zhong, Y. Wu, C. Schenck, F. Ng, M. Steigerwald, S. X. Xiao, C. Nuckolls, *Acc. Chem. Res.* **2015**, *48*, 267 – 276.
[46] Y.-F. Li, Y. Cao, J. Gao, D.-L. Wang, G. Yu, A. Heeger, *Synth. Met.* **1999**, *99*, 243 – 248.
[47] G. Zhang, C. B. Musgrave, *J. Phys. Chem. A* **2007**, *111*, 1554 – 1561.
[48] A. Heeger, *J. Adv. Mater.* **2014**, *26*, 10 – 28.
[49] Y. Ito, A. A. Virkar, S. Mannsfeld, J. H. Oh, M. Toney, J. Locklin, Z. N. Bao, *J. Am. Chem. Soc.* **2009**, *131*, 9396 – 9404.

Manuscript received: May 16, 2016
Accepted Article published: June 16, 2016
Final Article published: July 15, 2016